*Desalination and Water Treatment*
www.deswater.com

doi: 10.5004/dwt.2023.29594

295 (2023) 150–165
May

# Bioceramic hydroxyapatite derived from waste bone for copper bioadsorption application using process optimization: solution for sustainability

Mouna Mekki[a,b], Khira Zlaoui Riahi[a], Karima Horchani-Naifer[a], Dorra Jellouli Ennigrou[a,*]

[a]*Physical Chemistry Laboratory of Mineral Materials and their Applications, National Center for Research in Materials Sciences, Technopark Borj Cedria, P.O. Box: 73-8027, Soliman, Tunisia, Tel.: (+216) 79 32 52 50/(+216) 79 32 52 80; Fax: (+216) 79 32 53 14; emails: ennigrou2@gmail.com (D.J. Ennigrou), mouna.mekki@fst.utm.tn (M. Mekki), khira.zlaoui@gmail.com (K.Z. Riahi), karima_horchani@yahoo.com (K. Horchani-Naifer)*
[b]*Faculty of Sciences of Tunis, Tunisia*

Received 25 October 2022; Accepted 18 April 2023

**ABSTRACT**

Novel natural hydroxyapatite was synthesized from fish bones via alkaline heat treatment to remove copper ions in an aqueous solution through adsorption process. The synthesized biomaterial was characterized by X-ray diffraction, Fourier-transform infrared spectroscopy, scanning electron microscopy, energy-dispersive X-ray spectroscopy and thermogravimetric analysis. The central composite design was employed to investigate the individual and synergistic effects of the experimental parameters of the adsorption process. The results suggest that the kinetics adsorption were well proved by pseudo-second-order models and the maximum adsorption capacity of Cu(II) was 28.97 mg·g$^{-1}$ at the ambient via the Langmuir model. The thermodynamic results also indicate that the adsorption processes are endothermic, feasible and spontaneous. Based on the analysis of variance, the results show a highly significant model and an excellent correlation ($R^2$ = 0.986) between the experimental and the predicted results of copper ion adsorption. Regeneration studies have shown that ethylenediaminetetraacetic acid can be used as a leaching solution for the adsorption of Cu(II) ions from natural hydroxyapatite (N-HAp). The analyzed results indicated that the synthesized N-HAp was an effective and promising material for the removal of Cu(II) ions.

*Keywords:* Biomaterial; Heavy metals; Response surface methodology; Recycling; Bioadsorption

## 1. Introduction

The study of potentially toxic elements (PTEs), such as heavy metals, and their negative impact on the environment and human health is an issue of great concern. These elements are highly toxic, non-degradable and easily transferable into food chains [1]. Heavy metals are commonly released from various sources such as metal plating facilities, mining operations, paper industries and pesticides [2].

However, the scientific community has focused on controlling and removing heavy metals from waste streams.

In this regard, numerous methods have been used to remove the heavy metals from an aqueous solution such as ion-exchange [3], reverse osmosis [4], adsorption [5], electrodialysis [6], ultrafiltration [7] and solvent extraction [8].

Among various treatment methods, adsorption is one of the most successful approaches in the field of separation technology, particularly in wastewater treatment processes. This is due to its considerable effectiveness such as simplicity of design, operation, as well as high separation efficiencies when compared to other methods. In the last three decades, many solid materials (adsorbents) have been employed to remove aqueous phase inorganics/organics (heavy metal

* Corresponding author.

ions, dyes). Recently, various adsorbents, currently used for heavy metal ions including activated carbon [9], clay material [10], zeolites [11], and biosorbents [12], which have been extracted from various industrial effluents [13].

In order to devise a more eco-friendly method at lower cost, hydroxyapatite (HAp) has been easily extractable from various animal sources, such as clam shells, cuttlefish bones, bovine bones [14], corals, fish bones and camel bones [15]. It has shown great efficiency in the adsorption and retention of heavy metals available in wastewater [16].

Accordingly, several types of research have been conducted on the extraction of natural hydroxyapatite (N-HAp) via different methods like calcination, alkaline hydrothermal hydrolysis, and polymer-assisted [17,18]. Compared to the commercial hydroxyapatite ($Ca_{10}(PO_4)_6(OH)_2$), N-HAp is not stoichiometric as it contains trace elements such as $Na^+$, $Zn^{2+}$, $Mg^{2+}$, $K^+$, $Si^{2+}$, $Ba^{2+}$, $F^-$ and $CO_3^{2-}$. The calcium/phosphorus ratio in N-HAp is higher than that of commercial apatite materials, making it more suitable for medical applications [19,20]. Furthermore, N-HAp is better than the synthetic one [17], which is embodied by highly biocompatibility [21], osteoconductivity [22], non-toxic, non-inflammatory, and non-immunogenic agent.

In addition, the crystal structure and chemical composition provide high crystal lattice flexibility which allows the exchange of $OH^-$, $PO_4^{3-}$ and $Ca^{2+}$ ions to accommodate anions and cations with different sizes and charges, such as heavy metal ions [23]. As a result of its strong adsorptive properties (big surface area, high stability, enhanced active sites and abundant functional groups), it has been increasingly used in the treatment of wastewater and nuclear waste [24].

On the other hand, among the abundant animal waste in Tunisia, fish wastes represent a huge biomaterial potential [25]. Recent statistics, indicate that aquaculture production in Tunisia has increased from 2,600 tons in 2005 to almost 21,900 tons in 2017 [26]. Among the processed fish, about 50% to 75% of the total quantity is discarded as waste. Therefore, the development of a recovery process for this waste has become a prominent necessity in Tunisia [25].

This study purposes to valorize a biomaterial as a natural source of N-HAp, through a treatment process of fish bone waste collected from the local fish market of Tunis. This product was characterized by several analytical methods and subsequently compared to commercial hydroxyapatite (C-HAp). Then, it has been used as abio-adsorbent for the removal of Cu(II) from an aqueous solution by batch adsorption.

In order to investigate the optimal conditions and the interaction between the most significant parameters such as initial concentration of Cu(II) ions, contact time, pH and adsorbent dose in the absorption, a central composite design (CCD) with response surface methodology (RSM) has been used. The adsorption data has been processed by isothermal, kinetic and thermodynamic studies for the purpose of determining the physico-chemical nature of the adsorption process.

## 2. Materials and methods

Commercial hydroxyapatite ($Ca_5(PO_4)_3OH$) has been provided by Chemische Fabrik Budenheim, Germany. Copper(II) sulfate pentahydrate ($CuSO_4{\cdot}5H_2O$, AR, 99%), sodium chloride (NaCl), ethylenediaminetetraacetic acid (EDTA) and hydrochloric acid (HCl) (37%) have been purchased from Sigma-Aldrich (Germany). Potassium hydroxide (KOH), sodium hydroxide (NaOH) and potassium nitrate ($KNO_3$) have been bought from Chemicals Developing Manufactory, Germany. A Milli-Q water purification system has been employed to prepare the solutions.

### 2.1. Synthesis of natural hydroxyapatite

Fresh fish bones wastes (Nazali, thon and sardine) were collected from the local fish market in Tunis City. Firstly, fish bones were separated from the meat and washed with hot distilled water several times and then stored in the refrigerators.

N-HAp was synthesized from fish bone by simple alkaline heat treatment, the cleaned fish bone was treated with 0.1 M NaOH solution at 60°C and a stirring rate of 150 rpm for 2 h (solid to liquid ratio was 1:50 $g{\cdot}mL^{-1}$). Then, it was washed with ultrapure water to remove some impurities [22]. Bones were dried at 60°C for 48 h in an oven and milled to particle sizes by the Vibratory Disc Mill (RS 200, Retsch, Germany) at 1,000 rpm for 5 min. Subsequently, the powder of bone was placed in silica crucible and calcined at 900°C using a heating rate 5°C/min with 2 h holding time in a muffle furnace to remove organic substance and avoid microbial contamination. The final product N-HAp is used as a bioadsorbent of heavy metal from wastewater.

### 2.2. Characterization of hydroxyapatite

The crystalline phase composition, diffraction lines of N-HAp and C-HAp were analyzed using X-ray diffraction (D8 Advance, Bruker, USA) with Cu-Kα radiation at 40 kV and 40 mA with a 2θ range of 0°–80°. Purity and functional groups of N-HAp were measured using Fourier-transform infrared spectroscopy in a Frontier FTIR/FIR Spectrometer, Model PerkinElmer (France) coupled with an accessory for working in attenuated total reflectance (ATR) in the range of 4,000–400 $cm^{-1}$. Thermogravimetric analysis (TGA/DSC$^{3+}$ Mettler Toledo, France) was carried out using a thermal analyzer to study the reactions and phase transition of the sample during the heating process from 25°C of 1,000°C at a heating rate of 10°C/min in air atmosphere. The surface morphology of N-HAp and C-HAp powders was examined by scanning electron microscopy analysis SEM (Philips Scanning Electron Microscope XL30 FEG, Eindhoven, The Netherlands). Energy-dispersive X-ray coupled with SEM performed the elementary analyses. The granule size of the sample was characterized using Microtrac S3500 Laser Granulometry, Germany. The point of zero charge values ($pH_{pzc}$) of the fish bones was determined using 0.1 M $KNO_3$ in initial pH adjusted from 2 to 12 by the addition of KOH or $HNO_3$. After equilibration, final pH values ($pH_f$) were measured once again. $pH_{pzc}$ were determined from the plateau of $pH_f = f(pH_i)$ plots [27].

### 2.3. Batch adsorption experiments

For batch adsorption of copper, adsorbents (0.05 g) were accurately weighed into a 50 mL conical flask. Then, 25 mL

of copper solution (50 mg·L$^{-1}$) was added and pH of the solution was adjusted and shaken by a multi-station magnetic stirrer at 250 rpm.

In order to study the optimum conditions for the batch adsorption, various experimental parameters were varied such as the effects of pH, which ranged from 2 to 8, adsorbent dosage 1–4 g·L$^{-1}$, initial concentration 10–120 mg·L$^{-1}$, contact time between solid–liquid 0–120 min and temperature from 25°C to 80°C.

After a period of steering, the sorbents were filtered. The final concentration of Cu(II) was measured by atomic absorption spectrophotometer (AAS, Analytik Jena novAA® 400P, Germany).

The removal percentage (R%) and the adsorbed amounts of metal ions $q_e$ (mg·L$^{-1}$) at equilibrium were calculated using Eqs. (1) and (2), respectively [28]:

$$\%\text{Romoval} = \frac{\left(C_i - C_e\right)}{C_i} \times 100 \tag{1}$$

$$q_e = \frac{\left(C_i - C_e\right)V}{C_i} \tag{2}$$

where $C_i$ and $C_e$ are the initial and equilibrium concentration of Cu(II) (mg·L$^{-1}$), respectively. $V$ is the volume of the copper solution (L) and $W$ is the amount (g) of the sorbent used in the reaction mixture.

### 2.4. Experimental design and optimization

Experimental design involves statistical modelling; more factors are varied to observe their effects on the results. The main purpose's to elicit the greatest amount of information by conducting the smallest number of experiments [29,30].

In this study, preliminary experiments were carried out to investigate the effect of the most influential factors on the adsorption process. CCD was used to investigate the individual and synergistic effects of the four independent variables: the initial Cu(II) concentration ($X_1$), contact time ($X_2$), pH ($X_3$) and dose of sorbent ($X_4$). Therefore, the $2^4$ factorial design is associated with a second-order polynomial model and is composed of sixteen trials completed by five replicates of the central point and eight axial points which are located at α distance from the center and make the design rotatable (α = 2). The actual values of the independent variables and their corresponding coded values (–α, –1, 0, +1, +α) are presented in Table 1. Experiments were performed in a random order (Table 1) and the optimized conditions were determined using spherical response surfaces given by a second-order polynomial model [Eq. (3)] [31].

$$Y(\%) = b_0 + \sum_{i=1}^{4} b_i X_i + \sum_{i=1}^{4} b_{ii} X_i^2 + \sum_{j=i+1}^{4} b_{ij} X_i X_j \tag{3}$$

where $Y$ (%) is the removal rate of metal adsorbed, $b_0$ is the constant value, $b_i$ is the regression coefficients for linear, $b_{ii}$ is the second-order main effect, and $b_{ij}$ is the second-order main effect, $X_i$ and $X_j$ are the independent variables.

The statistical analysis of the CCD experimental results, response surface modeling and optimization of process variables were carried out using NEMROD-W Version 9901 D Software.

### 2.5. Desorption experiments

In order to investigate the reversibility of $Cu^{2+}$ sorption, desorption experiments using different leaching solutions were realized. Firstly, fish bone particles were loaded with $Cu^{2+}$ by equilibrating the adsorbent with $2 \times 10^{-3}$ mol·L$^{-1}$ of $Cu^{2+}$ solution. The resulting suspensions were separated and the final metals concentrations were analyzed. Subsequently, the solid residue was rinsed several times with distilled water in order to remove desorbed metal ions attached to the bone surface and dried at 50°C [32].

Secondly, 0.1 g of the obtained adsorbents were added to 20 mL of three kinds of leaching solutions including, pH 4 with 0.01 M NaCl, 0.003 M EDTA, and 0.01 M HCl, respectively at 25°C ± 1°C under steering for 24 h. Finally, after leaching, the solutions were filtered and the metal concentrations in each leaching solution were measured by AAS [33].

## 3. Results and discussion

### 3.1. Characterization of hydroxyapatite

The natural hydroxyapatite (N-HAp) obtained from fish bone is described as follows and compared with C-HAp. The X-ray diffraction (XRD) are represented in Fig. 1 and used to observe the phase compositions of N-HAp, which refers to standard hydroxyapatite (COD reference: PDF 01-074-0566). The characteristic peaks of the N-HAp are located at 2θ = 25.9°, 28.9°, 31.8°, 32.2°, 32.9°, 39.8°, 46.7°, 49.5° and 50.5°, corresponding to the (002), (210), (211), (112), (300), (130), (222), (213), and (321) planes, respectively. It's clear that the normalized data of the standard hydroxyapatite (PDF 01-074-0566) coincides exactly with the apparent diffraction peaks; suggesting that the high crystallinity of N-HAp has been produced and it matches with the hexagonal structure of apatite standard. Furthermore, no new characteristic peak of N-HAp appeared after $Cu^{2+}$ adsorption, but there was a slight shift in the peak compared with the N-HAp pattern before adsorption (Fig. 1a) and the XRD reflection of the standard hydroxyapatite (Fig. 1d). These results can be explained by the possibility of $Ca^{2+}$ ions (0.99 Å) with

Table 1
Experimental range, actual and coded values of the independent test factors

| Factors | Levels | | | Star point | |
|---|---|---|---|---|---|
| | –1 | 0 | +1 | –α | +α |
| $X_1$: Cu(II) concentration (mg·L$^{-1}$) | 37.500 | 65.000 | 92.500 | 10.000 | 120.000 |
| $X_2$: contact time (min) | 45 | 70 | 95 | 20 | 120 |
| $X_3$: pH | 3.25 | 4.5 | 5.75 | 2 | 7 |
| $X_4$: adsorbent dose (g·L$^{-1}$) | 1.75 | 2.5 | 3.25 | 1 | 4 |

larger radius in HAp being replaced by $Cu^{2+}$ ions (0.72 Å), suggesting that the $Cu^{2+}$ adsorption mechanism by N-HAp involves ion-exchange with $Ca^{2+}$ [34].

Fig. 2 shows the FTIR spectra of N-HAp compared to commercial hydroxyapatite C-HAp. The stretching vibration bands of –OH groups in both hydroxyapatites (N-HAp and C-HAp), are found between 3,343 and 3,546 $cm^{-1}$ [35]. The band at 1,049 $cm^{-1}$ is assigned by $\nu_1$ P–O stretching vibration and the band at 955 $cm^{-1}$ is attributed to $\nu_2$ O–P–O bending vibrations. The bands at 606 and 564 $cm^{-1}$ correspond to $\nu_3$ O–P–O bending vibration and the band at 467 $cm^{-1}$ is due to the $\nu_4$ symmetric P–O stretching vibration [36]. The vibrational bands $[PO_4]^{3-}$ depend on the activation temperature. In addition, characteristics of vibrations bands of the C–O in the carbonate group were observed at 1,431–1,440 $cm^{-1}$ [37].

Fig. 3a shows the results of the TGA curve of the C-HAp which present two steps of weight loss. The first step in order of 4.23 wt.%, observed between 50°C and 400°C, is associated with the decomposition of residual species such as nitrogenous compounds, hydrocarbons or the water constituting the non-reacted reagents. The second step close to 1.06 wt.%, in the range of 650°C–750°C, is related to the partial dehydroxylation of hydroxyapatite to oxyhydroxyapatite $Ca_{10}(PO_4)_6O$.

Fig. 3b shows the TGA curve of the waste fish bone sample before calcination, the result indicates that there are two steps of weight loss that occur during the heating process for the waste fish bone sample. The first weight loss of 12.2 wt.%, was observed from 70°C to 250°C due to the elimination of trapped water in the bone. The second weight loss of about 21.1 wt.% was realized from 260°C to 620°C and due to the decomposition of organic components, such as collagen and protein in the bone structure. There is also a very small weight loss (1%) in the range of 800°C–950°C. This implies that the organic components have been removed and the remaining phase is N-HAp, which proves the XRD analysis [38].

On the other hand, Fig. 4 represents the N-HAp particle distribution. The result shows that the average particle size $d(50)$ and maximum size $d(95)$ of N-HAp are 14.81 and 65 μm, respectively.

The SEM micrograph of C-HAp and N-HAp are illustrated in Fig. 5. This figure displays irregular-shaped particles with a pores structure in the C-HAp, however, N-HAp

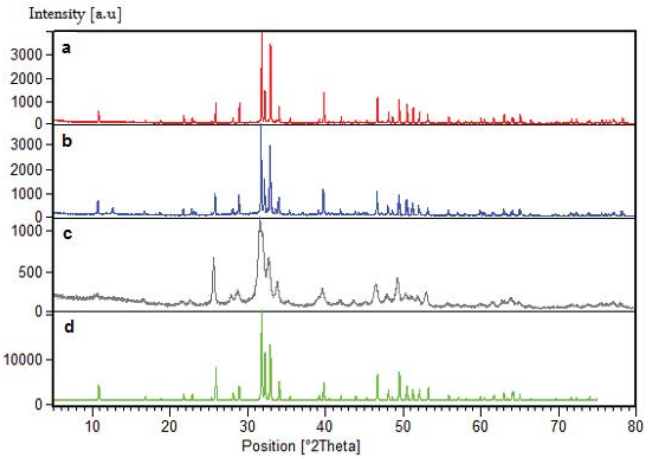


Fig. 1. X-ray diffraction pattern of the natural hydroxyapatite before (a), after adsorption (b), commercial hydroxyapatite (c) and standard hydroxyapatite (d).

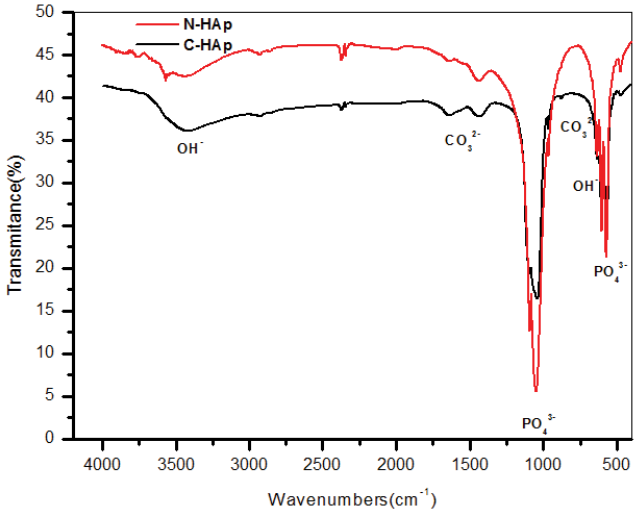


Fig. 2. Fourier-transform infrared spectra for commercial hydroxyapatite and natural hydroxyapatite.

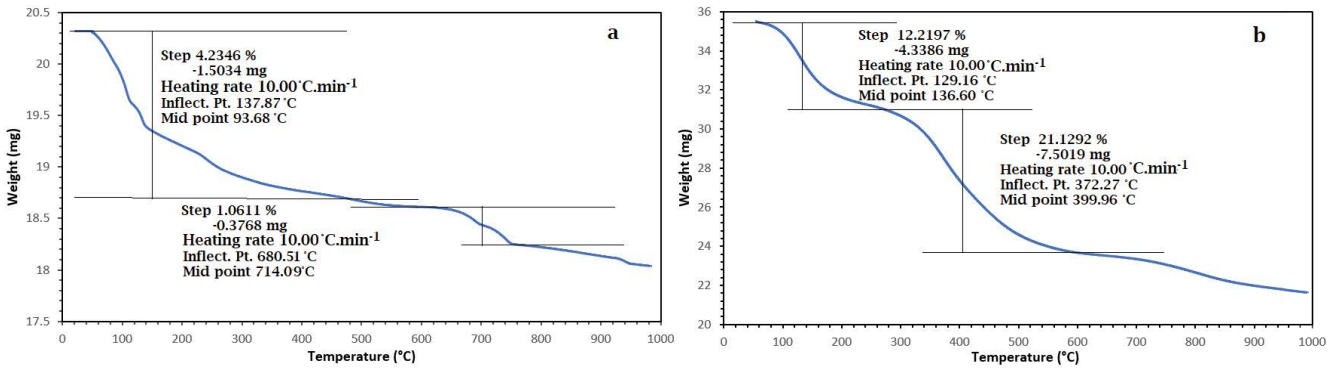


Fig. 3. Thermogravimetric analysis curve of the commercial hydroxyapatite (a) and waste fish bone sample before calcination (b) heated from 25°C to 1,000°C.

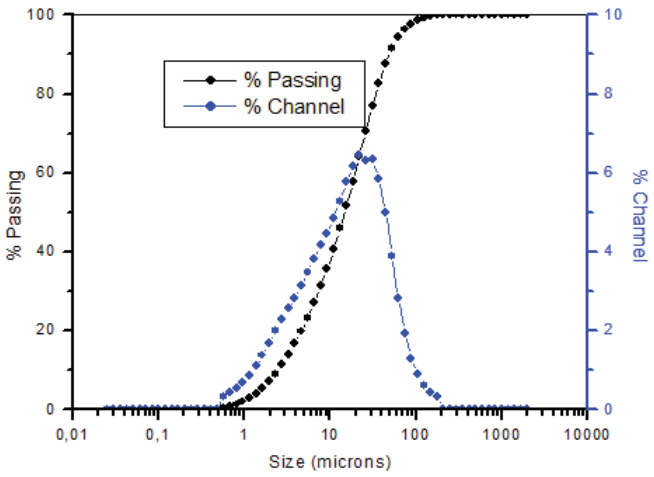


Fig. 4. Average natural hydroxyapatite particle size.

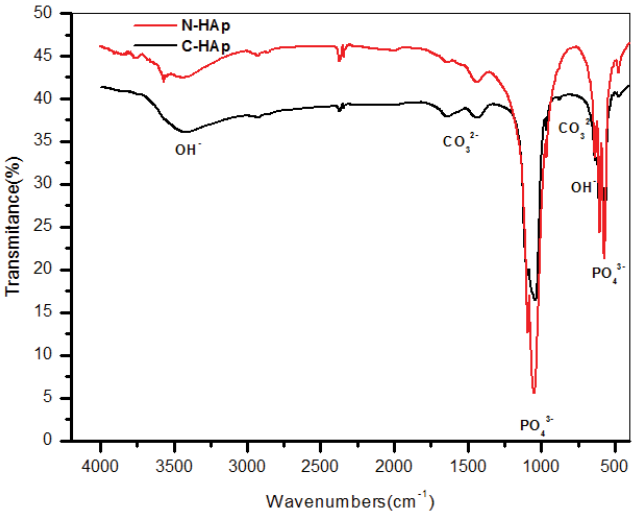


Fig. 5. Scanning electron micrograph and energy-dispersive X-ray spectroscopy analysis of commercial hydroxyapatite and natural hydroxyapatite.

sample shows a large number of agglomerated non-uniform spherical particles [39].

Compared to C-HAp, the N-HAp particles are larger and form a more porous structure. A highly porous structure is likely to be a significant factor for the performance of N-HAp as an adsorbent.

According to energy-dispersive X-ray spectroscopy (EDX) analysis (Fig. 5), the N-HAp samples have a significant amount of the main elements for the crystalline structure of hydroxyapatite which are O, P and Ca [35].

The N-HAp presents significant peaks at 3.71 and 2.02 keV illustrating that the Ca/P molar ratio of the N-HAp was 1.71 (25.5 at.% Ca and 14.90 at.% P) is very close to the theoretical value (1.67) that is similar to the value of the Ca/P molar ratio for C-HAp. These results are consistent with a previous report [40]. These obtained results indicate that the synthesized compound presents a great purity. Furthermore, N-HAp post-adsorption is dried at 50°C

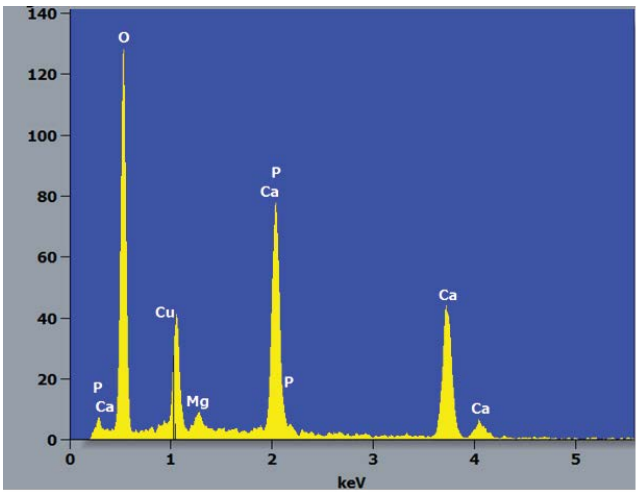


Fig. 6. Energy-dispersive X-ray spectroscopy analysis of natural hydroxyapatite after adsorption.

overnight, and then the chemical compositions are determined by EDX (Fig. 6). The results show the appearance of a new peak corresponding to copper ions.

The zero-charge point ($pH_{pzc}$) of material relies on the chemical and electronic properties of the functional groups appearing on its surface [41]. Fig. 7 represents the zero charge point of N-HAp, which is determined by measuring the $pH_f$ in the function of $pH_0$. The $pH_{pzc}$ is evaluated to be 9.5. Therefore, at $pH_{solution} < pH_{pzc}$, proton consumption occurs via protonation of the surface functional groups (≡Ca–$OH^0$ and ≡P–$O^-$), which repels positively charged Cu(II) away from the positively charged ≡Ca–$OH_2^+$ and ≡P–OH groups, leading to an increase in the $pH_f$. Furthermore, at a $pH_{solution} > pH_{pzc}$, the surface charge of N-HAp can become negative due to the consumption of $OH^-$ through deprotonation of the surface functional groups (≡Ca–$OH_2^+$ and ≡P–OH). It leads to the enhancement of the $pH_f$ and predominance of neutral ≡Ca–$OH^0$ and negatively charged ≡P–$O^-$ which promotes the attractive electrostatic interaction between positively charged Cu(II) and the negatively charged N-HAp surface [42].

### 3.2. Batch adsorption studies: kinetic study

In order to understand the mechanism and dynamism of adsorption, three kinetic models have been chosen as pseudo-first-order [Eq. (4)] [43], pseudo-second-order [Eq. (5)] and intraparticle diffusion [Eq. (6)] [44]. These models are described in linear forms by Eqs. (4)–(6) [45].

$$\ln\left(q_e - q_t\right) = \ln q_e - k_1 t \tag{4}$$

$$\frac{t}{q_t} = \left(\frac{1}{k_2 q_e^2}\right) + \left(\frac{t}{q_e}\right) \tag{5}$$

$$q_t = K_{id} t^{1/2} + C \tag{6}$$

where $q_e$ and $q_t$ are the amounts of metal ions adsorbed on the hydroxyapatite (mg·g$^{-1}$) at equilibrium and at time $t$. $K_1$

($min^{-1}$) and $K_2$ ($g \cdot mg^{-1} \cdot min^{-1}$) are the first-order rate constant and the second-order rate constant, respectively. $K_{id}$ ($mg \cdot g^{-1} \cdot min^{-1/2}$) and $C$ are the intraparticle diffusion rate constant and intercept, respectively.

The effect of contact time on the removal of copper ions by N-HAp was studied at pH = 5.5, 50 $mg \cdot L^{-1}$ Cu(II) concentration, and 2 $g \cdot L^{-1}$ adsorbent dose. The samples were obtained at different times from 0 to 180 min. The experimental data of the kinetics study has been shown in supplementary Fig. S1.

The rate removal of Cu(II) was increased significantly during the initial phase up to 90 min to reach 87.88%, then it remains constant until reaching the equilibrium (Fig. S1a).

Table 2 represents the determined rate constants and corresponding correlation coefficient constants ($R^2$). According to the findings of these three kinetic models, the theoretical adsorption capacity ($q_{e,cal}$ = 22.727 $mg \cdot g^{-1}$) calculated by pseudo-second-order model is similar to the experimental data ($q_{e,exp}$ = 20.526 $mg \cdot g^{-1}$), with a correlation coefficient near to 1 ($R^2$ = 0.998). These results suggest that the adsorption of Cu(II) by natural hydroxyapatite can be explained from two aspects [46]:

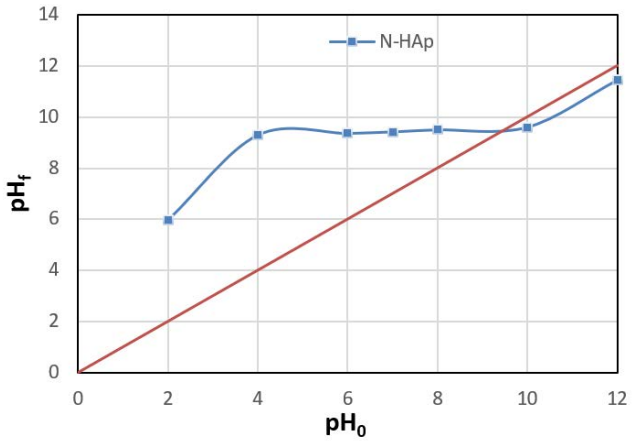


Fig. 7. $pH_{pzc}$ of natural hydroxyapatite.

Table 2
Kinetic parameters of Cu(II) removal

| Kinetic models | Step | Parameters | Values |
|---|---|---|---|
| First-order | – | $q_e$ ($mg \cdot g^{-1}$) | 19.433 |
| | | $K_1$ ($min^{-1}$) | 0.032 |
| | | $R^2$ | 0.989 |
| Second-order | – | $q_e$ ($mg \cdot g^{-1}$) | 22.727 |
| | | $K_2$ ($g \cdot mg^{-1} \cdot min^{-1}$) | $0.227 \times 10^{-2}$ |
| | | $R^2$ | 0.998 |
| Intraparticle diffusion | Step 1 | $K_{id1}$ ($mg \cdot g^{-1} \cdot min^{-1/2}$) | 2.685 |
| | | $R^2$ | 0.999 |
| | | $C_1$ | –1.132 |
| | Step 2 | $K_{id2}$ ($mg \cdot g^{-1} \cdot min^{-1/2}$) | 1.690 |
| | | $R^2$ | 0.991 |
| | | $C_2$ | 3.749 |
| | Step 3 | $K_{id3}$ ($mg \cdot g^{-1} \cdot min^{-1/2}$) | 0.031 |
| | | $R^2$ | 0.997 |
| | | $C_3$ | 20.193 |

Firstly, an ion-exchange reaction between $Ca^{2+}$ and $Cu^{2+}$ in an aqueous solution at pH 5 and 6, as confirmed by the XRD analyses and EDX of N-HAp post-adsorption. Their mechanism could be described as follows [Eq. (7)]:

$$Ca_{10}(PO_4)_6(OH)_2 + xCu^{2+} \rightarrow Ca_{10-x}Cu_x(PO_4)_6(OH)_2 + xCa^{2+} \quad (7)$$

The second is that N-HAp dissolves in an acidic aqueous solution, releasing phosphate, which reacts with Cu(II) (dissolution–precipitation mechanism). Generally, hydroxyapatite has a dominant solubility at low pH, the dissolved phosphate binds to Cu(II) to form Cu-apatite ($Cu_{10}(PO_4)_6X_2$), wherein $X$ is a monovalent anion depending on the presence or absence of $OH^-$, $Cl^-$ and $F^-$ in solution. In this study, the dissolution–precipitation mechanism could be expressed as follows [Eqs. (8) and (9)]:

$$Ca_{10}(PO_4)_6(OH)_2 + 14H^+ \rightarrow 10Ca^{2+} + 6H_2PO_4^- + 2H_2O \quad (8)$$

$$10Cu^{2+} + 6H_2PO_4^- + 2H_2O \rightarrow Cu_{10}(PO_4)_6(OH)_2 + 14H^+ \quad (9)$$

To control the intraparticle mass transport inside the adsorbent, the intraparticle diffusion model is adopted (Fig. 8). Based on the shape of the curve $q_t$ as a function of $t^{1/2}$, the plot does not pass through the origin ($C \neq 0$) and exhibits a multi-linearity relationship, indicating that intraparticle diffusion is not the only rate determining step [42]. In addition, the following three portions presented in the curve (Fig. 8) could explain the linear fitting results of the intraparticle diffusion model indicating the Cu(II) adsorption process. The first step corresponds to boundary layer diffusion or external surface adsorption, about 10 min. The second step is a gradual adsorption stage attributed to intraparticle diffusion, about 90 min. The third plateau region is equilibrium adsorption [47]. Therefore, the intraparticle process might be another rate limiting step for the removal of Cu(II) by N-HAp.

### 3.3. Isotherm adsorption study

Isotherm adsorption models are employed to describe the adsorption behaviors when the adsorption process reaches an equilibrium state. The Langmuir model is given by Eq. (10):

$$\frac{C_e}{q_e} = \frac{1}{q_m K_L} + \left(\frac{1}{q_m}\right) C_e \quad (10)$$

where $q_e$ ($mg \cdot g^{-1}$), is the amount of metal adsorbed per unit of N-HAp at equilibrium; $C_e$ is the residual metal concentration in solution at equilibrium ($mg \cdot L^{-1}$); $q_m$ is the theoretical monolayer maximum adsorption capacity and $K_L$ ($L \cdot mg^{-1}$) is the Langmuir constant related to the affinity of the binding sites (energy of adsorption).

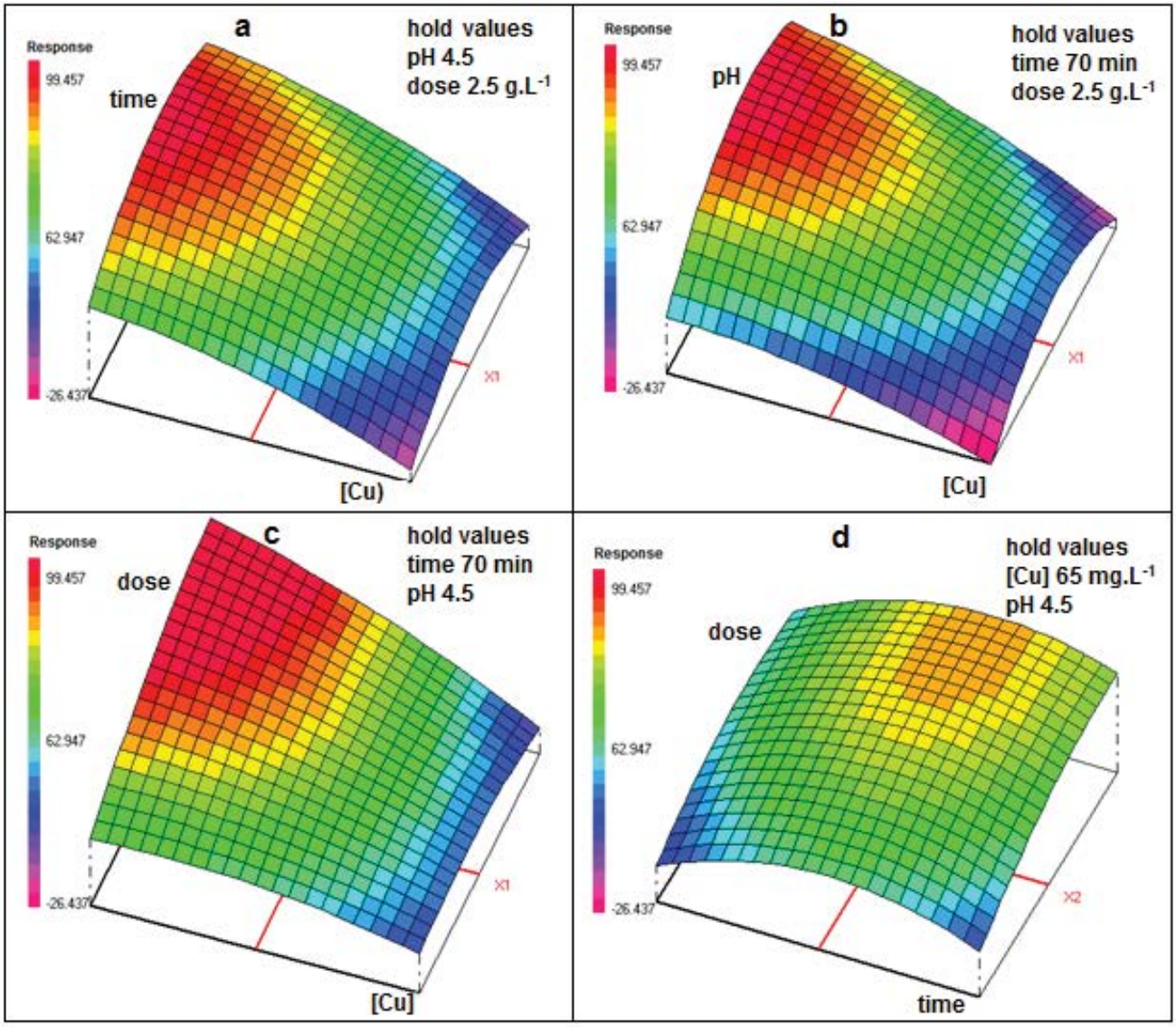


Fig. 8. Optimization plots for the predicted percentage removal of copper ions.

The Freundlich model is presented by the following equation [48]:

$$\log q_e = \log K_F + \frac{1}{n}\log C_e \tag{11}$$

where $K_F$ (L·mg$^{-1}$) is the Freundlich constant related to the adsorption capacity, and $n$ is the Freundlich constant related to adsorption intensity.

An alternative model used to investigate the adsorption process is developed by Temkin [Eq. (12)]:

$$q_e = \frac{RT}{B}\ln K_T + \frac{RT}{B}\ln C_e \tag{12}$$

where $R$ is the ideal gas constant (8.314 J·mol$^{-1}$·K$^{-1}$), $T$ (K) is the absolute temperature, $K_T$ (L·mg$^{-1}$) and $B$ (J·mol$^{-1}$) are Temkin parameters related to the equilibrium binding and the heat of adsorption, respectively.

The last isothermal model used is suggested by Dubinin–Radushkevich shown in Eq. (13):

$$\ln q_e = \ln q_s - K_{DR}\varepsilon^2 \left(\varepsilon = RT\left(1+\frac{1}{C_e}\right)\right) \tag{13}$$

where $K_{DR}$ (mol$^2$·kJ$^{-2}$) is Dubinin–Radushkevich isotherm constant related to the mean free energy of adsorption, e is the Polanyi potential and $q_s$ (mol·g$^{-1}$) is the theoretical saturation capacity [49,50].

Mean energy of adsorption per mole of adsorbate $E$ (kJ·mol$^{-1}$) and the interactions involved in the process of adsorption are presented in Eq. (14):

$$E = \frac{1}{\sqrt{2K_{DR}}} \tag{14}$$

According to the results highlighted in supplementary Fig. S2 and the experimental data summarized in

Table 3, it can be concluded that the Langmuir isotherm models ($R^2$ = 0.992) appear to be the most accurate model and provides a better description for the equilibrium data [51]. This result suggests that the adsorption of Cu(II) onto the N-HAp can be attributed to energetically homogeneous binding sites on the adsorbent surface with monolayer coverage of Cu(II) following adsorption [45].

Based on the previous result presented by the Langmuir model, the maximum monolayer adsorption capacities of the adsorbents N-HAp to remove Cu(II) predicted by the Langmuir isotherm model ($q_{m,\text{cal}}$ = 28.99 mg·g$^{-1}$) is close to the experimental values ($q_{m,\text{exp}}$ = 28.82 mg·g$^{-1}$). From the Freundlich isotherm plots ($0 < 1/n < 0.5$), it could be deduced that Cu(II) is easily adsorbed on N-HAp [46]. It could be concluded that the adsorption of Cu(II) is compatible to Langmuir isotherm model, which is in accordance with other researches [51,52]. Furthermore, the model [Eq. (14)] allows the distinction between chemical and physical adsorption processes when evaluating parameter $E$. For the values of $E$ < 8 kJ·mol$^{-1}$, shows the physical adsorption however 8 < $E$ < 16 kJ·mol$^{-1}$ indicates ion-exchange mechanism and $E$ > 16 kJ·mol$^{-1}$ suggests the chemical nature of adsorption [53,54]. According to Table 3 the value of $E$ (5 kJ·mol$^{-1}$) suggests that the interaction between the copper ions and the adsorbent is essentially due to physical attractions.

### 3.4. Thermodynamic analysis

The thermodynamic parameters such as the Gibbs free energy ($\Delta G°$), standard enthalpy ($\Delta H°$) and entropy ($\Delta S°$) of adsorption could help to explain the inherent energetic changes involved in the sorption process [55].

The changes in thermodynamic parameters are calculated using the following equations:

$$\ln K_d = \frac{\Delta\text{Sads}}{R} - \frac{\Delta\text{Hads}}{RT} \tag{15}$$

Table 3
Isotherms parameters and correlation coefficients calculated for the Cu(II) adsorption on natural hydroxyapatite at 25°C

| Models | Parameters | Values |
|---|---|---|
| Langmuir | $R^2$ | 0.992 |
| | $q_{m,\text{cal}}$ (mg·g$^{-1}$) | 28.986 |
| | $K_L$ (L·mg$^{-1}$) | 0.506 |
| | $R_L$ | 0.016–0.165 |
| Freundlich | $R^2$ | 0.956 |
| | 1/$n$ | 0.222 |
| | $K_F$ (mg·g$^{-1}$) | 12.167 |
| Temkin | $R^2$ | 0.986 |
| | $B$ (J·mol$^{-1}$) | 3.314 |
| | $K_T$ (L·mg$^{-1}$) | 1.646 |
| Dubinin–Radushkevich | $R^2$ | 0.898 |
| | $q_s$ (mol·g$^{-1}$) | 23.306 |
| | $K_{\text{DR}}$ (mol$^2$·J$^{-2}$) | 2 × 10$^{-8}$ |
| | $E$ (kJ·mol$^{-1}$) | 5 |

$$\Delta G = \Delta\text{Hads} - T\Delta\text{Sads} \tag{16}$$

The distribution coefficient $K_d$ (L·g$^{-1}$) of adsorption is defined as:

$$K_d = \frac{q_e}{C_e} \tag{17}$$

The parameters $\Delta H°$ and $\Delta S°$ were determined from the slope and intercept of the plots of ln$K_d$ vs. 1/$T$ (Fig. S3) and the values are listed in Table 4. The negative $\Delta G$ values indicate the feasibility and spontaneous adsorption process of copper on the bioadsorbent hydroxyapatite. Moreover, the positive value of $\Delta S$ indicates that the randomness at the solid/solution interface increase during the adsorption process [56,57]. Also, the positive values of $\Delta H$ indicate an endothermic nature of adsorption. This endothermic nature might be associated with the Cu(II) ions solvation and desolvation. Heavy metal ions need to be barred from their hydration sheaths to some extent before adsorption onto N-HAp and as a result, the endothermicity of the desolvation process overwhelms the exothermicity of Cu(II) ions adsorption to the surface of N-HApX [39]. The magnitude of $\Delta H$ has given an indication on the type of biosorption, which could be either physical or chemical. If the heat of biosorption is between 2.1 and 20.9 kJ·mol$^{-1}$, then the process is physical and if it is between 20.9 and 418.4 kJ·mol$^{-1}$, the process is chemical [58]. In the present study, the standard enthalpy value is 22.05 kJ·mol$^{-1}$, which is closer to the limit value of the domain corresponding to physisorption (between 2.1 and 20.9 kJ·mol$^{-1}$). Based on experimental errors that will be considered and the calculation of mean free energy of Dubinin–Radushkevich isotherm value ($E$ = 5 kJ·mol$^{-1}$), it is noticed that the adsorption of Cu(II) ions on N-HAp is a physisorption process.

### 3.5. Response surface methodology study

A central composite design was used to optimize the maximum adsorption of Cu(II). Table 5 represents the experimental conditions, values obtained and predicted via the CCD for Cu(II) removal from aqueous solutions.

The optimum conditions of the parameters such as $X_1$ (Cu(II) concentration), $X_2$ (contact time), $X_3$ (pH) and $X_4$ (adsorbent dosage) on the removal of copper ions $Y$ (%) are optimized and found to be 37.5 mg·L$^{-1}$, 95 min, 5.7 and 3.25 g·L$^{-1}$, respectively.

Table 4
Thermodynamic parameters for Cu(II) adsorption on natural hydroxyapatite

| Temperature (K) | $K_d$ (L·mg$^{-1}$) | $\Delta G°$ (kJ·mol$^{-1}$) | $\Delta H°$ (kJ·mol$^{-1}$) | $\Delta S°$ (J·mol$^{-1}$·K$^{-1}$) |
|---|---|---|---|---|
| 298.15 | 1.211 | –0.103 | 22.05 | 74.30 |
| 308.15 | 1.231 | –0.846 | – | – |
| 318.15 | 1.589 | –1.589 | – | – |
| 333.15 | 2.922 | –2.729 | – | – |
| 353.15 | 4.253 | –4.189 | – | – |

Table 5
Experimental conditions, values obtained and predicted via the central composite design for Cu(II) removal from aqueous solutions

| Runs | Factors | | | | Responses | | |
|---|---|---|---|---|---|---|---|
| | $X_1$ | $X_2$ | $X_3$ | $X_4$ | $Y_{exp}$ (%) | $Y_{cal}$ (%) | Residual |
| 1 | 37.5 | 45.00 | 3.25 | 1.75 | 29.626 | 28.574 | 1.052 |
| 2 | 92.5 | 45.00 | 3.25 | 1.75 | 5.907 | 7.952 | –2.045 |
| 3 | 37.5 | 95.00 | 3.25 | 1.75 | 36.977 | 35.233 | 1.744 |
| 4 | 92.5 | 95.00 | 3.25 | 1.75 | 7.833 | 10.100 | –2.267 |
| 5 | 37.5 | 45.00 | 5.75 | 1.75 | 57.080 | 53.809 | 3.271 |
| 6 | 92.5 | 45.00 | 5.75 | 1.75 | 21.272 | 20.338 | 0.934 |
| 7 | 37.5 | 95.00 | 5.75 | 1.75 | 67.613 | 65.831 | 1.782 |
| 8 | 92.5 | 95.00 | 5.75 | 1.75 | 25.026 | 27.849 | –2.823 |
| 9 | 37.5 | 45.00 | 3.25 | 3.25 | 62.359 | 61.392 | 0.966 |
| 10 | 92.5 | 45.00 | 3.25 | 3.25 | 9.885 | 13.794 | –3.908 |
| 11 | 37.5 | 95.00 | 3.25 | 3.25 | 70.696 | 73.576 | –3.060 |
| 12 | 92.5 | 95.00 | 3.25 | 3.25 | 16.517 | 21.646 | –5.129 |
| 13 | 37.5 | 45.00 | 5.75 | 3.25 | 81.683 | 81.542 | 0.140 |
| 14 | 92.5 | 45.00 | 5.75 | 3.25 | 17.493 | 21.094 | –3.601 |
| 15 | 37.5 | 95.00 | 5.75 | 3.25 | 99.457 | 99.269 | 0.188 |
| 16 | 92.5 | 95.00 | 5.75 | 3.25 | 31.132 | 34.310 | –3.179 |
| 17 | 10 | 70.00 | 4.50 | 2.5 | 92.766 | 97.799 | –5.034 |
| 18 | 120 | 70.00 | 4.50 | 2.5 | 21.235 | 21.218 | 9.017 |
| 19 | 65 | 20.00 | 4.50 | 2.5 | 24.624 | 25.020 | –0.396 |
| 20 | 65 | 120.00 | 4.50 | 2.5 | 49.275 | 44.895 | 4.380 |
| 21 | 65 | 70.00 | 2.00 | 2.5 | 6.742 | 2.408 | 4.332 |
| 22 | 65 | 70.00 | 7.00 | 2.5 | 39.959 | 40.307 | –0.348 |
| 23 | 65 | 70.00 | 4.50 | 1 | 30.344 | 33.160 | –2.816 |
| 24 | 65 | 70.00 | 4.50 | 4 | 79,238 | 72.439 | 6.710 |
| 25 | 65 | 70.00 | 4.50 | 2.5 | 68,781 | 68.186 | 0.595 |
| 26 | 65 | 70.00 | 4.50 | 2.5 | 67.157 | 68.186 | –1.029 |
| 27 | 65 | 70.00 | 4.50 | 2.5 | 68.981 | 68.186 | 0.795 |
| 28 | 65 | 70.00 | 4.50 | 2.5 | 68.506 | 68.186 | 0.320 |
| 29 | 65 | 70.00 | 4.50 | 2.5 | 67.507 | 68.186 | –0.679 |

According to the multiple regression analysis on the design matrix and the responses given in Table 5, the following second-order polynomial equations in the coded form are determined to show the effects of independent factors on the removal rate [Eq. (18)]:

$$Y = 68.186 - 21.395X_1 + 4.969X_2 + 9.475X_3 + 9.820X_4 - 3.295X_1^2 - 8.307X_2^2 - 11.707X_3^2 - 3.847X_4^2 - 1.128X_1X_2 - 3.212X_1X_3 + 1.341X_2X_3 - 6.744X_1X_4 + 1.426X_2X_4 - 1.271X_3X_4 \quad (18)$$

The positive coefficient signs indicate a synergistic effect while the negative indicate an antagonistic effect [59]. Also, the model equations and regression coefficients are significant ($P < 0.01$) and must be included in the model. The percentage removal of Cu(II) related with all factors was studied.

Table 6
Estimated regression coefficient for adsorption of Cu(II)

| | Coefficient value | F. inflation | Standard deviation | *t*.exp | *p*-value |
|---|---|---|---|---|---|
| $b_0$ | 68.186 | | 0.361 | 188.81 | *** |
| $b_1$ | –21.395 | 1 | 0.165 | –129.80 | *** |
| $b_2$ | 4.969 | 1 | 0.165 | 30.14 | *** |
| $b_3$ | 9.475 | 1 | 0.165 | 57.48 | *** |
| $b_4$ | 9.820 | 1 | 0.165 | 59.57 | *** |
| $b_{11}$ | –3.295 | 1.08 | 0.189 | –20.78 | *** |
| $b_{22}$ | –8.307 | 1.08 | 0.189 | –52.40 | *** |
| $b_{33}$ | –11.707 | 1.08 | 0.189 | –73.85 | *** |
| $b_{44}$ | –3.847 | 1.08 | 0.189 | –24.27 | *** |
| $b_{12}$ | –1.128 | 1 | 0.202 | –5.59 | ** |
| $b_{13}$ | –3.212 | 1 | 0.202 | –15.91 | *** |
| $b_{23}$ | 1.341 | 1 | 0.202 | 6.64 | ** |
| $b_{14}$ | –6.744 | 1 | 0.202 | –33.41 | *** |
| $b_{24}$ | 1.426 | 1 | 0.202 | 7.06 | ** |
| $b_{34}$ | –1.271 | 1 | 0.202 | –6.30 | ** |

***Extremely significant

In fact, the student's statistical *t*-test for analysis of variance (Nemrod W) was used to confirm the above experimental design and validate the statistical model by determining the significance of the regression coefficients. In addition, the *p*-value was determined to indicate the test's significance (Table 6).

To evaluate these models, the determined correlation coefficient $R^2$ is 0.986, which implies validation of most of the data variations by the regression model obtained. The $R^2$ value could be fitted by the adjusted $R^2_{adj}$ value (0.971) for the number of terms and sample size in the model. It is noted that this value is slightly different from the multiple $R^2$. These values indicate that the quadratic model could be predicted by the impact of the independent variables on the Cu(II) removal efficiency [60]. The $R^2_{pred}$ value (0.92) determined by cross-validation suggests that the model could be explained by a variation in predicting novel observations [61].

In addition, the analysis of variance is the most important condition to validate and confirm the significance of the model [62]. According to Table 7, when the *p*-value (<0.01) the quadratic model is highly significant. Indeed, the $F_{tab}$ (10.4.5%) = 5.96 < *F*-value (47.575) indicates that the non-significant lack of fit factor could be justified and significant since it is greater than 0.05. These results validate and confirm the significant CCD model.

### 3.6. Adsorbent response surface plots for copper removal as functions of binary effects

Three-dimensional (3D) response surface plots were used to determine the function of two factors at the same time, holding the other component at the zero level, to provide a better explanation of the effects of the independent variables and their interactions.

Table 7
Analysis of variance for central composite design

| | Sum of square (SS) | Degree of freedom | Mean square | *F*-value | *p*-value |
|---|---|---|---|---|---|
| Regression | 21,614.8 | 14 | 1,543.91 | 2,367.663 | <0.01*** |
| Residual | 312.839 | 14 | 22.346 | | |
| Lack of fit | 310.230 | 10 | 31.023 | 47.575 | ** |
| Error | 2.608 | 4 | 0.652 | | |
| Total | 21,927.6 | 28 | | | |

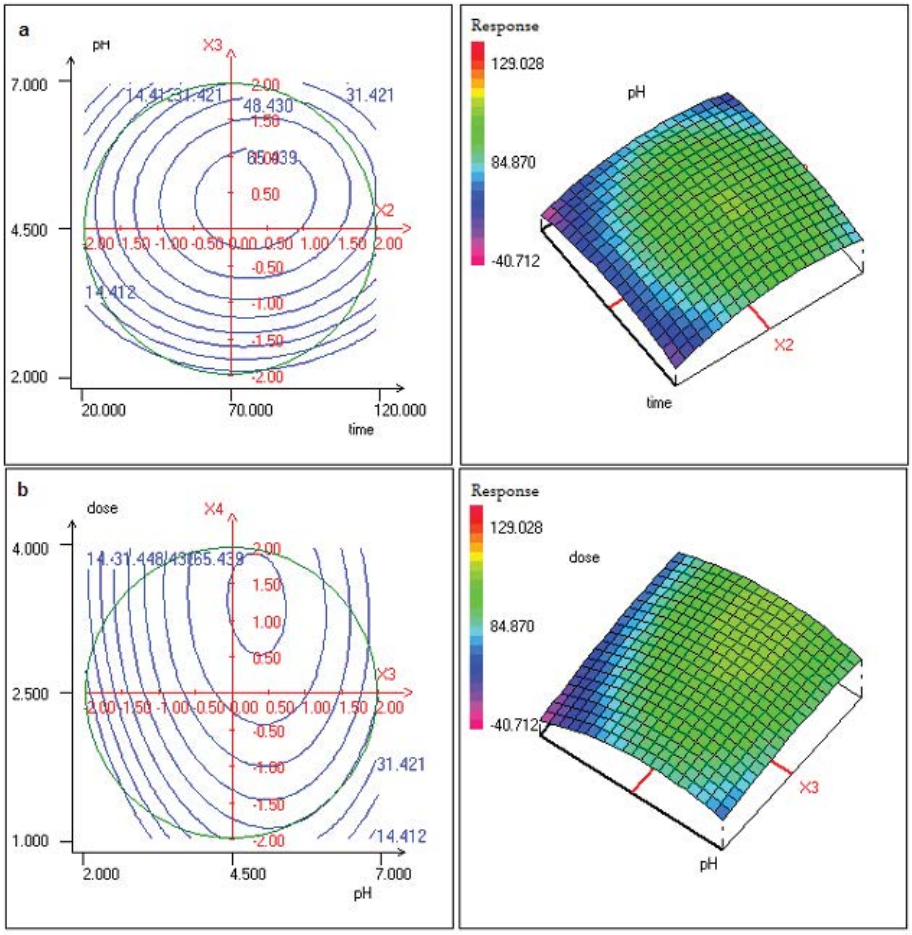


Fig. 9. Response surface plots for Cu(II) removal by adsorption process as a function of initial pH and contact time (a) and use a function of adsorbent dose and initial pH (b) (ions concentration = 65 mg·L$^{-1}$).

Fig. 8 demonstrates the effect of significant interactions between the four factors ($X_1$: ions concentration, $X_2$: contact time, $X_3$: pH of solution, $X_4$: adsorbent dose) in order to adsorb copper ions by N-HAp.

Based on Fig. 8a, the optimal removal of Cu(II) is observed during 76 min with a value pH 4.5, Cu(II) concentration 10.652 mg·L$^{-1}$ and an adsorbent dose 2.5 g·L$^{-1}$.

In addition, plots of ion concentration vs. pH level reveal that the best parameters for maximum copper removal are obtained when the adsorbent dose and contact time are set at 2.5 g·L$^{-1}$ and 70 min, respectively and the pH level is between 4.7 and 5.7, and the Cu(II) concentration is

Table 8
Desorption of Cu(II) from natural hydroxyapatite

| Eluting agent | Initial pH | Final pH | Desorbed Cu(II) (%) |
|---|---|---|---|
| Hydrochloric acid (HCl) (0.01 M) | 2.41 | 5.3 | 2.3 |
| Ethylenediaminetetraacetic acid (EDTA) (0.003 M) | 4.87 | 5.6 | 89 |
| Sodium chloride (NaCl) (0.01 M) | 4.15 | 5.71 | 0.01 |

Table 9
Comparative study for removal of copper ions by different adsorbents

| Adsorbents | Maximum sorption capacity ($mg \cdot g^{-1}$) | References |
|---|---|---|
| Chitosan/hydroxyapatite/nano-magnetite ($Fe_3O_4$) composite | 3.656 | [16] |
| Fe–Mn oxide/zeolite | 58.56 | [65] |
| Walnut shell ash | 29 | [66] |
| Natural hydroxyapatite/chitosan composite | 1.776 | [67] |
| Unmodified lemon peel | 13.2 | [68] |
| Sodium alginate/polyvinyl alcohol/kaolin/polyacrylamide (SA/PVA/K/PAM) | 5.061 | [69] |
| Natural hydroxyapatite | 28.82 | This study |

18.806 $mg \cdot L^{-1}$ (Fig. 8b). Thus, during 70 min at a pH fixed at 4.5, a removal rate of copper ions reaches 99%, when the dose of the adsorbent is above 2.5 $g \cdot L^{-1}$ and with a Cu(II) concentration between 10 and 40 $mg \cdot L^{-1}$ (Fig. 8c). The increase in Cu(II) removal effectiveness with increased N-HAp dosage is due to an increase in the number of free accessible adsorption sites [63]. Also, for Fig. 8d, by setting the copper concentration to 65 $mg \cdot L^{-1}$ and the solution pH to 4.5, the response surface of the Cu(II) ion removal plot shows a better Cu(II) removal efficiency when the N-HAp dose is 2.5 $g \cdot L^{-1}$ for treatment duration between 68 and 92 min.

Similarly, for the 2D and 3D response surface plots of the binary effect between solution pH and contact time and between solution pH and adsorbent dose for the Cu(II) removal, shows that the optimal conditions for maximum Cu(II) elimination are precisely inside the design limit (Fig. 9). In this step, the concentration of Cu(II) and the dose of the adsorbent are fixed at 65 $mg \cdot L^{-1}$ and 2.5 $g \cdot L^{-1}$, respectively. The maximum of Cu adsorption is obtained when the solution pH is ranged between 4.2 and 5.9, while the contact time is in the range of 59 and 99 min (Fig. 9a). Similarly, the concentration of Cu(II) and the contact time were fixed at 65 $mg \cdot L^{-1}$ and 70 min, respectively. Based on the above, it can be deduced that the efficiency of copper ion removal is high when the initial pH of the copper solution ranges from 4.43 to 5.4 and the dose of adsorbent ranges from 2.9 to 3.9 $g \cdot L^{-1}$ (Fig. 9b).

According to the results obtained previously from the theoretical study, the optimal values of the tested factors influencing the experience are the following: ions concentration of 18.06 $mg \cdot L^{-1}$, contact time of 70 min, initial pH of 5.2 and adsorbent dose of 2.5 $g \cdot L^{-1}$, while the maximum of copper removal (%) predicted is about 99.46%.

### 3.7. Desorption experiment

Table 8 shows the results of the desorption studies. It can be observed that the efficiency of Cu(II) desorption from N-HAp depends on the extracting solution. Due to the development of a complex between EDTA and metal ions, the amount of Cu(II) desorbed from the EDTA solution is the highest. In addition, when the acidic solution is used, the desorbed amount of copper ions decreases.

The N-HAp has relatively low desorption efficiency of heavy metal ions, similar to previous studies [64].

In addition, the low desorption efficiency of N-HAp inhibited copper ion's movement in natural water. As a result, it could be an efficient adsorbent for copper pollution treatment, particularly in lightly polluted water.

### 3.8. Comparative study

The performance of different adsorbents on the adsorption of copper ions from an aqueous solution has been evaluated, and their maximum adsorption capacities ($q_m$) were compared to those reported in previous literature (Table 9). The results showed that N-HAp had a higher performance compared to other adsorbents in terms of $q_m$ or feasibility. However, some composite adsorbents are more performing, but their synthesis process was found to be costly and complex. Therefore, considering the economic cost and application field, N-HAp appears to have better prospects for adsorption.

## 4. Conclusions

N-HAp as a bioadsorbent is synthesized by recycling waste fish bone, using simple alkaline heat treatment, in order to remove copper ions from an aqueous solution via the adsorption process. To prove the structure and constituent elements of the resulting product, several methods were employed. Various experimental parameters (pH, initial concentration of Cu(II), contact time, adsorbent dose and temperature) are examined to evaluate the adsorption process. Therefore, the kinetic study is determined and fitted by pseudo-second-order model. The Langmuir model with a high correlation coefficient is effective since it provides a better fit to the isothermal data. In addition, the results of the thermodynamic study show that the adsorption process is endothermic, feasible and spontaneous. An experimental design methodology based on central composite design is used to investigate the impact of various experimental parameters on the removal of Cu(II). The results demonstrate that the optimal conditions for Cu(II) adsorption are as follows: initial Cu(II) concentration 37.5 $mg \cdot L^{-1}$, pH 5.75, contact time 95 min and adsorbent dose 3.25 $g \cdot L^{-1}$ with a removal rate reaching 99.46%. The validation of the RSM model confirms its adequacy in optimizing the adsorption process and that the regression equations could be used as a theoretical basis for the retention of heavy metals from wastewater by adsorption treatment. Furthermore, for the copper(II) ions desorption, EDTA is proved to be the most selective leaching solution. These results suggest that N-HAp could be a suitable adsorbent for Cu(II) removal. However,

practical application to wastewater and the removal of other metals should also be further investigated.

### Credit author statement

M. Mekki: Study development, Empirical discussion, Data, Methodology, and Estimations. K. Zlaoui Riahi: Analyses. K. Horchani-Naifer: Manuscript development. D. Jellouli Ennigrou: Manuscript development and Proofreading.

### Declaration of competing interest

The authors declare that they have no known competing financial interests or personal relationships that could have appeared to influence the work reported in this paper.

### Acknowledgements

We are thankful to National Center for Research in Materials Sciences, Technopark Borj Cedria, Tunisia for their financial support of this work.

### Funding

This work was supported by the Ministry of Higher Education and Scientific Research, Tunisia.

### Symbols

| | | |
|---|---|---|
| $b_0$ | — | Constant value of the model |
| $b_i$ | — | Regression coefficients for linear |
| $b_{ii}$ | — | Second-order main effect |
| $b_{ij}$ | — | Second-order main effect of the *i*-factor and *j*-factor |
| $C$ | — | Intraparticle diffusion intercept |
| $C_e$ | — | Residual metal concentration in solution at equilibrium, mg·L$^{-1}$ |
| $C_i$ | — | Initial concentration of Cu(II), mg·L$^{-1}$ |
| $d$ | — | Particle size of the powder |
| $E$ | — | Free energy, kJ·mol$^{-1}$ |
| $K_1$ | — | First-order rate constant, min$^{-1}$ |
| $F_{tab}$ | — | Value of the *F* distribution table |
| *F*-value | — | Value of the *F* distribution |
| $K_2$ | — | Second-order rate constant, g·mg$^{-1}$·min$^{-1}$ |
| $K_d$ | — | Distribution coefficient of adsorption, L·g$^{-1}$ |
| $K_{DR}$ | — | Dubinin–Radushkevich isotherm constant related to the mean free energy of adsorption, mol$^2$ kJ$^{-2}$ |
| $K_F$ | — | Freundlich constant related to the adsorption capacity |
| $K_{id}$ | — | Intraparticle diffusion rate constant, mg·g$^{-1}$·min$^{-1/2}$ |
| $K_L$ | — | Langmuir constant related to the affinity of the binding sites, L·mg$^{-1}$ |
| $K_T$ | — | Temkin parameters related to the heat of adsorption |
| $n$ | — | Freundlich constant related to adsorption intensity |
| $P$ | — | Regression coefficients of the model equation |
| $pH_f$ | — | Final pH values |
| $pH_i$ | — | Initial pH values |
| $pH_{pzc}$ | — | Zero charge point |
| $q_e$ | — | Amount of metal adsorbed per unit of N-HAp at equilibrium, mg·g$^{-1}$ |
| $q_{e,cal}$ | — | Theoretical adsorption capacity, mg·g$^{-1}$ |
| $q_{e,exp}$ | — | Experimental adsorption capacity, mg·g$^{-1}$ |
| $q_m$ | — | Theoretical monolayer maximum adsorption capacity, mg·g$^{-1}$ |
| $q_s$ | — | Theoretical saturation capacity, mol·g$^{-1}$ |
| $q_t$ | — | Amounts of metal ions adsorbed on the hydroxyapatite at time, mg·g$^{-1}$ |
| $R$ | — | Ideal gas constant, 8.314 J·mol$^{-1}$·K$^{-1}$ |
| $R^2$ | — | Correlation coefficient |
| $R^2_{adj}$ | — | Correlation coefficient adjusted |
| $R^2_{pred}$ | — | Correlation coefficient predicted |
| $T$ | — | Absolute temperature, K |
| $t^{1/2}$ | — | Half-reaction time |
| $V$ | — | Volume of the copper solution, L |
| $W$ | — | Amount of the sorbent used in the reaction mixture, g |
| $X_i$ | — | Level of the *i*-factor |
| $X_j$ | — | Level of the *j*-factor |
| $X_iX_j$ | — | Product of the *i*-factor and *j*-factor |
| $Y$(%) | — | Experimental model response: removal rate of metal adsorbed |
| $\Delta G°$ | — | Gibbs free energy |
| $\Delta H°$ | — | Standard enthalpy |
| $\Delta S°$ | — | Entropy thermodynamic parameter |
| α | — | Distance from center and make the design rotatable |
| Θ | — | Angle of reflection of X-rays in XRD, degrees |
| e | — | Polanyi adsorption potential |
| $\nu_1$ | — | P–O stretching vibration at 1,049 cm$^{-1}$ |
| $\nu_2$ | — | O–P–O bending vibrations at 955 cm$^{-1}$ |
| $\nu_3$ | — | O–P–O bending vibration at 606 and 564 cm$^{-1}$ |
| $\nu_4$ | — | Symmetric P–O stretching vibration at 467 cm$^{-1}$ |

### References

[1] F. Khelifi, A. Melki, Y. Hamed, P. Adamo, A.G. Caporale, Environmental and human health risk assessment of potentially toxic elements in soil, sediments, and ore-processing wastes from a mining area of southwestern Tunisia, Environ. Geochem. Health, 42 (2020) 4125–4139.

[2] F. Fu, Q. Wang, Removal of heavy metal ions from wastewaters: a review, J. Environ. Manage., 92 (2011) 407–418.

[3] L. Yang, Z. Wei, W. Zhong, J. Cui, W. Wei, Modifying hydroxyapatite nanoparticles with humic acid for highly efficient removal of Cu(II) from aqueous solution, Colloids Surf., A, 490 (2016) 9–21.

[4] B. Alyüz, S. Veli, Kinetics and equilibrium studies for the removal of nickel and zinc from aqueous solutions by ion-exchange resins, J. Hazard. Mater., 167 (2009) 482–488.

[5] H.-J. Choi, S.-W. Yu, Application of novel hybrid bioadsorbent, tannin/chitosan/sericite, for the removal of Pb(II) toxic ion from aqueous solution, Korean J. Chem. Eng., 35 (2018) 2198–2206.

[6] C.S.L. dos Santos, M.H. Miranda Reis, V.L. Cardoso, M.M. de Resende, Electrodialysis for removal of chromium(VI) from effluent: analysis of concentrated solution saturation, J. Environ. Chem. Eng., 7 (2019) 103380, doi: 10.1016/j.jece.2019.103380.

[7] S.-Y. Tang, Y.-R. Qiu, Removal of copper(II) ions from aqueous solutions by complexation–ultrafiltration using rotating disk membrane and the shear stability of PAA–Cu complex, Chem. Eng. Res. Des., 136 (2018) 712–720.
[8] Y. Li, L. Yang, Z. Xu, Q. Sun, Separation and recovery of heavy metals from wastewater using synergistic solvent extraction, IOP Conf. Ser.: Mater. Sci. Eng., 167 (2017) 012005, doi: 10.1088/1757-899X/167/1/012005.
[9] M. Kobya, E. Demirbas, E. Senturk, M. Ince, Adsorption of heavy metal ions from aqueous solutions by activated carbon prepared from apricot stone, Bioresour. Technol., 96 (2005) 1518–1521.
[10] A. Sdiri, T. Higashi, R. Chaabouni, F. Jamoussi, Competitive removal of heavy metals from aqueous solutions by montmorillonitic and calcareous clays, Water Air Soil Pollut., 223 (2012) 1191–1204.
[11] M. Irannajad, H. Kamran Haghighi, Removal of heavy metals from polluted solutions by zeolitic adsorbents: a review, Environ. Processes, 8 (2021) 7–35.
[12] B.-S. Liaw, T.-T. Chang, H.-K. Chang, W.-K. Liu, P.-Y. Chen, Fish scale-extracted hydroxyapatite/chitosan composite scaffolds fabricated by freeze casting—an innovative strategy for water treatment, J. Hazard. Mater., 382 (2020) 121082, doi: 10.1016/j.jhazmat.2019.121082.
[13] M. Wang, K. Zhang, M. Wu, Q. Wu, J. Liu, J. Yang, J. Zhang, Unexpectedly high adsorption capacity of esterified hydroxyapatite for heavy metal removal, Langmuir, 35 (2019) 16111–16119.
[14] R. Bazargan-Lari, M.E. Bahrololoom, A. Nemati, Z. Salehi, Adsorption of Cu(II) ions from industrial wastewater on natural hydroxyapatite extracted from bone ash, J. Food Agric. Environ., 9 (2011) 652–657.
[15] A. Esmaeilkhanian, F. Sharifianjazi, A. Abouchenari, A. Rouhani, N. Parvin, M. Irani, Synthesis and characterization of natural nano-hydroxyapatite derived from Turkey femur-bone waste, Appl. Biochem. Biotechnol., 189 (2019) 919–932.
[16] A. Pooladi, R. Bazargan-Lari, Simultaneous removal of copper and zinc ions by chitosan/hydroxyapatite/nano-magnetite composite, J. Mater. Res. Technol., 9 (2020) 14841–14852.
[17] S.M.H. Dabiri, A.A. Rezaie, M. Moghimi, H. Rezaie, Extraction of hydroxyapatite from fish bones and its application in nickel adsorption, BioNanoScience, 8 (2018) 823–834.
[18] N.A.S. Mohd Pu'ad, P. Koshy, H.Z. Abdullah, M.I. Idris, T.C. Lee, Syntheses of hydroxyapatite from natural sources, Heliyon, 5 (2019) e01588, doi: 10.1016/j.heliyon.2019.e01588.
[19] M. Akram, R. Ahmed, I. Shakir, W.A.W. Ibrahim, R. Hussain, Extracting hydroxyapatite and its precursors from natural resources, J. Mater. Sci., 49 (2014) 1461–1475.
[20] D. Milovac, T.C. Gamboa-Martínez, M. Ivankovic, G. Gallego Ferrer, H. Ivankovic, PCL-coated hydroxyapatite scaffold derived from cuttlefish bone: *in-vitro* cell culture studies, Mater. Sci. Eng., C, 42 (2014) 264–272.
[21] T. Varadavenkatesan, R. Vinayagam, S. Pai, B. Kathirvel, A. Pugazhendhi, R. Selvaraj, Synthesis, biological and environmental applications of hydroxyapatite and its composites with organic and inorganic coatings, Prog. Org. Coat., 151 (2021) 106056, doi: 10.1016/j.porgcoat.2020.106056.
[22] P. Shi, M. Liu, F. Fan, C. Yu, W. Lu, M. Du, Characterization of natural hydroxyapatite originated from fish bone and its biocompatibility with osteoblasts, Mater. Sci. Eng., C, 90 (2018) 706–712.
[23] S. Campisi, C. Castellano, A. Gervasini, Tailoring the structural and morphological properties of hydroxyapatite materials to enhance the capture efficiency towards copper(II) and lead(II) ions, New J. Chem., 42 (2018) 4520–4530.
[24] D.M. Imam, S.I. Moussa, M.F. Attallah, Sorption behavior of some radionuclides using prepared adsorbent of hydroxyapatite from biomass waste material, J. Radioanal. Nucl. Chem., 319 (2019) 997–1012.
[25] T. Kraiem, A.B. Hassen-Trabelsi, S. Naoui, H. Belayouni, M. Jeguirim, Characterization of the liquid products obtained from Tunisian waste fish fats using the pyrolysis process, Fuel Process. Technol., 138 (2015) 404–412.
[26] FAO: United States Food and Agriculture Organization, Fishery and Aquaculture Country Profiles, Tunisia, 2021. Available at: http://www.fao.org/fishery/facp/TUN/fr
[27] I. Smičiklas, A. Onjia, S. Raičević, Experimental design approach in the synthesis of hydroxyapatite by neutralization method, Sep. Purif. Technol., 44 (2005) 97–102.
[28] L. Yang, W. Zhong, J. Cui, Z. Wei, W. Wei, Enhanced removal of Cu(II) ions from aqueous solution by poorly crystalline hydroxyapatite nanoparticles, J. Dispersion Sci. Technol., 37 (2016) 956–968.
[29] Z. Alam, S.A. Muyibi, J. Toramae, Statistical optimization of adsorption processes for removal of 2,4-dichlorophenol by activated carbon derived from oil palm empty fruit bunches, J. Environ. Sci., 19 (2007) 674–677.
[30] H. Arslanoğlu, R. Orhan, M.D. Turan, Application of response surface methodology for the optimization of copper removal from aqueous solution by activated carbon prepared using waste polyurethane, Anal. Lett., 53 (2020) 1343–1365.
[31] M. Ghaedi, H.Z. Khafri, A. Asfaram, A. Goudarzi, Response surface methodology approach for optimization of adsorption of Janus Green B from aqueous solution onto $ZnO/Zn(OH)_2$-NP-AC: kinetic and isotherm study, Spectrochim. Acta, Part A, 152 (2016) 233–240.
[32] B. Kizilkaya, A.A. Tekinay, Y. Dilgin, Adsorption and removal of Cu(II) ions from aqueous solution using pretreated fish bones, Desalination, 264 (2010) 37–47.
[33] Y. Feng, J.-L. Gong, G.-M. Zeng, Q.-Y. Niu, H.-Y. Zhang, C.-G. Niu, J.-H. Deng, M. Yan, Adsorption of Cd(II) and Zn(II) from aqueous solutions using magnetic hydroxyapatite nanoparticles as adsorbents, Chem. Eng. J., 162 (2010) 487–494.
[34] Y. Chen, M. Li, Y. Li, Y. Liu, Y. Chen, H. Li, L. Li, F. Xu, H. Jiang, L. Chen, Hydroxyapatite modified sludge-based biochar for the adsorption of $Cu^{2+}$ and $Cd^{2+}$: adsorption behavior and mechanisms, Bioresour. Technol., 321 (2021) 124413, doi: 10.1016/j.biortech.2020.124413.
[35] A. Ramdani, A. Kadeche, M. Adjdir, Z. Taleb, D. Ikhou, S. Taleb, A. Deratani, Lead and cadmium removal by adsorption process using hydroxyapatite porous materials, Water Pract. Technol., 15 (2020) 130–141.
[36] D.-X. Guan, C. Ren, J. Wang, Y. Zhu, Z. Zhu, W. Li, Characterization of lead uptake by nano-sized hydroxyapatite: a molecular scale perspective, ACS Earth Space Chem., 2 (2018) 599–607.
[37] H.S.M. Abd-Rabboh, K.F. Fawy, N.S. Awwad, Removal of copper(II) from aqueous samples using natural activated hydroxyapatite sorbent produced from camel bones, Desal. Water Treat., 164 (2019) 300–309.
[38] F. Sharifianjazi, A. Esmaeilkhanian, M. Moradi, A. Pakseresht, M.S. Asl, H. Karimi-Maleh, H.W. Jang, M. Shokouhimehr, R.S. Varma, Biocompatibility and mechanical properties of pigeon bone waste extracted natural nano-hydroxyapatite for bone tissue engineering, Mater. Sci. Eng., B, 264 (2021) 114950, doi: 10.1016/j.mseb.2020.114950.
[39] A. Khawar, Z. Aslam, A. Zahir, I. Akbar, A. Abbas, Synthesis of Femur extracted hydroxyapatite reinforced nanocomposite and its application for Pb(II) ions abatement from aqueous phase, Int. J. Biol. Macromol., 122 (2019) 667–676.
[40] S. Kongsri, K. Janpradit, K. Buapa, S. Techawongstien, S. Chanthai, Nanocrystalline hydroxyapatite from fish scale waste: preparation, characterization and application for selenium adsorption in aqueous solution, Chem. Eng. J., 215–216 (2013) 522–532.
[41] A. Rathnayake, O. Hettithanthri, A.U. Rajapaksha, M. Vithanage, Preparation and Characterization of Dendro Biochar-Hydroxyapatite Composite: A Potential Material for Defluoridation, 2021 Moratuwa Engineering Research Conference (MERCon), Moratuwa, Sri Lanka, 2021, pp. 160–163.
[42] K.-W. Jung, S.Y. Lee, J.-W. Choi, Y.J. Lee, A facile one-pot hydrothermal synthesis of hydroxyapatite/biochar nanocomposites: adsorption behavior and mechanisms for the removal of copper(II) from aqueous media, Chem. Eng. J., 369 (2019) 529–541.

[43] H. Moussout, H. Ahlafi, M. Aazza, H. Maghat, Critical of linear and nonlinear equations of pseudo-first-order and pseudo-second-order kinetic models, Karbala Int. J. Mod. Sci., 4 (2018) 244–254.
[44] H. Herbache, A. Ramdani, A. Maghni, Z. Taleb, S. Taleb, E. Morallon, R. Brahmi, Removal of o-cresol from aqueous solution using Algerian Na-clay as adsorbent, Desal. Water Treat., 57 (2016) 20511–20519.
[45] Z. Zhang, X. Wang, H. Wang, J. Zhao, Removal of Pb(II) from aqueous solution using hydroxyapatite/calcium silicate hydrate (HAP/C-S-H) composite adsorbent prepared by a phosphate recovery process, Chem. Eng. J., 344 (2018) 53–61.
[46] L. Cui, Y. Wang, L. Hu, L. Gao, B. Du, Q. Wei, Mechanism of Pb(II) and methylene blue adsorption onto magnetic carbonate hydroxyapatite/graphene oxide, RSC Adv., 5 (2015) 9759–9770.
[47] S. Swamiappan, S. Ganesan, V. Sekar, S. Devaraj, A. Subramanian, V.K. Ponnusamy, P. Kathirvel, Effective removal of cationic methylene blue dye using nano-hydroxyapatite synthesized from fish scale bio-waste, Int. J. Appl. Ceram. Technol., 18 (2021) 902–912.
[48] R. Bazargan-Lari, M.E. Bahrololoom, A. Nemati, Sorption behavior of Zn(II) ions by low cost and biological natural hydroxyapatite/chitosan composite from industrial wastewater, J. Food Agric. Environ., 9 (2011) 892–897.
[49] Y. Liu, G. Zeng, L. Tang, Y. Cai, Y. Pang, Y. Zhang, G. Yang, Y. Zhou, X. He, Y. He, Highly effective adsorption of cationic and anionic dyes on magnetic Fe/Ni nanoparticles doped bimodal mesoporous carbon, J. Colloid Interface Sci., 448 (2015) 451–459.
[50] A. Babkin, I. Burakova, A. Burakov, D. Kurnosov, E. Galunin, A. Tkachev, I. Ali, Adsorption of $Cu^{2+}$, $Zn^{2+}$ and $Pb^{2+}$ ions on a novel graphene-containing nanocomposite: an isotherm study, IOP Conf. Ser.: Mater. Sci. Eng., 693 (2019) 012045, doi: 10.1088/1757-899X/693/1/012045.
[51] A. Phasuk, S. Srisantitham, T. Tuntulani, W. Anutrasakda, Facile synthesis of magnetic hydroxyapatite-supported nickel oxide nanocomposite and its dye adsorption characteristics, Adsorption, 24 (2018) 157–167.
[52] H. Hernández-Cocoletzi, R.A. Salinas, E. Águila-Almanza, E. Rubio-Rosas, W.S. Chai, K.W. Chew, C. Mariscal-Hernández, Pau Loke Show d, Natural hydroxyapatite from fishbone waste for the rapid adsorption of heavy metals of aqueous effluent, Environ. Technol. Innovation, 20 (2020) 101109, doi: 10.1016/j.eti.2020.101109.
[53] A. Bambaeero, R. Bazargan-Lari, Simultaneous removal of copper and zinc ions by low cost natural snail shell/hydroxyapatite/chitosan composite, Chin. J. Chem. Eng., 33 (2021) 221–230.
[54] Ç. Sarici-Özdemir, Y. Önal, Error analysis studies of dye adsorption onto activated carbon from aqueous solutions, Part. Sci. Technol., 32 (2014) 20–27.
[55] S. Meski, N. Tazibt, H. Khireddine, S. Ziani, W. Biba, S. Yala, D. Sidane, F. Boudjouan, N. Moussaoui, Synthesis of hydroxyapatite from mussel shells for effective adsorption of aqueous Cd(II), Water Sci. Technol., 80 (2019) 1226–1237.
[56] Y. Si, J. Huo, Y. Hengbo, A. Wang, Adsorption kinetics, isotherms, and thermodynamics of Cr(III), Pb(II), and Cu(II) on porous hydroxyapatite nanoparticles, J. Nanosci. Nanotechnol., 18 (2018) 3484–3491.
[57] M. Lu, Y. Zhang, X. Guan, X. Xu, T. Gao, Thermodynamics and kinetics of adsorption for heavy metal ions from aqueous solutions onto surface amino-bacterial cellulose, Trans. Nonferrous Met. Soc. China, 24 (2014) 1912–1917.
[58] S. Kondapalli, K. Mohanty, Influence of temperature on equilibrium, kinetic and thermodynamic parameters of biosorption of Cr(VI) onto fish scales as suitable biosorbent, J. Water Resour. Prot., 3 (2011) 429–439.
[59] G. Louhıchı, L. Bousselmı, A. Ghrabı, I. Khounı, Process optimization via response surface methodology in the physico-chemical treatment of vegetable oil refinery wastewater, Environ. Sci. Pollut. Res., 26 (2019) 18993–19011.
[60] M. Rastgordani, J. Zolgharnein, Simultaneous determination and optimization of Titan Yellow and Reactive Blue 4 dyes removal using chitosan@hydroxyapatite nanocomposites, J. Polym. Environ., 29 (2021) 1789–1807.
[61] M. Mäkelä, Experimental design and response surface methodology in energy applications: a tutorial review, Energy Convers. Manage., 151 (2017) 630–640.
[62] A. Akhtar, K. Akram, Z. Aslam, I. Ihsanullah, N. Baig, M.M. Bello, Photocatalytic degradation of p-nitrophenol in wastewater by heterogeneous cobalt supported ZnO nanoparticles: modeling and optimization using response surface methodology, Environ. Prog. Sustainable Energy, 42 (2023) e13984, doi: 10.1002/ep.13984.
[63] A. Javid, A. Roudbari, N. Yousefi, M.A. Fard, B. Barkdoll, S.S. Talebi, S. Nazemi, M. Ghanbarian, S.K. Ghadiri, Modeling of chromium(VI) removal from aqueous solution using modified green-graphene: RSM-CCD approach, optimization, isotherm, and kinetic studies, J. Environ. Health Sci. Eng., 18 (2020) 515–529.
[64] L. Dong, Z. Zhu, Y. Qiu, J. Zhao, Removal of lead from aqueous solution by hydroxyapatite/magnetite composite adsorbent, Chem. Eng. J., 165 (2010) 827–834.
[65] J. Lu, F. Zhang, Novel Fe–Mn oxide/zeolite composite material for rapid removal of toxic copper ions from aqueous solutions, J. Cleaner Prod., 397 (2023) 136496, doi: 10.1016/j.jclepro.2023.136496.
[66] R. Foroutan, S.J. Peighambardoust, R. Mohammadi, S.H. Peighambardoust, B. Ramavandi, Development of new magnetic adsorbent of walnut shell ash/starch/$Fe_3O_4$ for effective copper ions removal: treatment of groundwater samples, Chemosphere, 296 (2022) 133978, doi: 10.1016/j.chemosphere.2022.133978.
[67] R. Bazargan-Lari, H.R. Zafarani, M.E. Bahrololoom, A. Nemati, Removal of Cu(II) ions from aqueous solutions by low-cost natural hydroxyapatite/chitosan composite: equilibrium, kinetic and thermodynamic studies, J. Taiwan Inst. Chem. Eng., 45 (2014) 1642–1648.
[68] S. Meseldzija, J. Petrovic, A. Onjia, T. Volkov-Husovic, A. Nesic, N. Vukelic, Utilization of agro-industrial waste for removal of copper ions from aqueous solutions and mining-wastewater, J. Ind. Eng. Chem., 75 (2019) 246–252.
[69] H. Huang, Q. Yang, C. Huang, L. Zhang, Facile and low-cost fabrication of composite hydrogels to improve adsorption of copper ions, Environ. Technol. Innovation, 27 (2022) 102427, doi: 10.1016/j.eti.2022.102427.

**Supporting information**

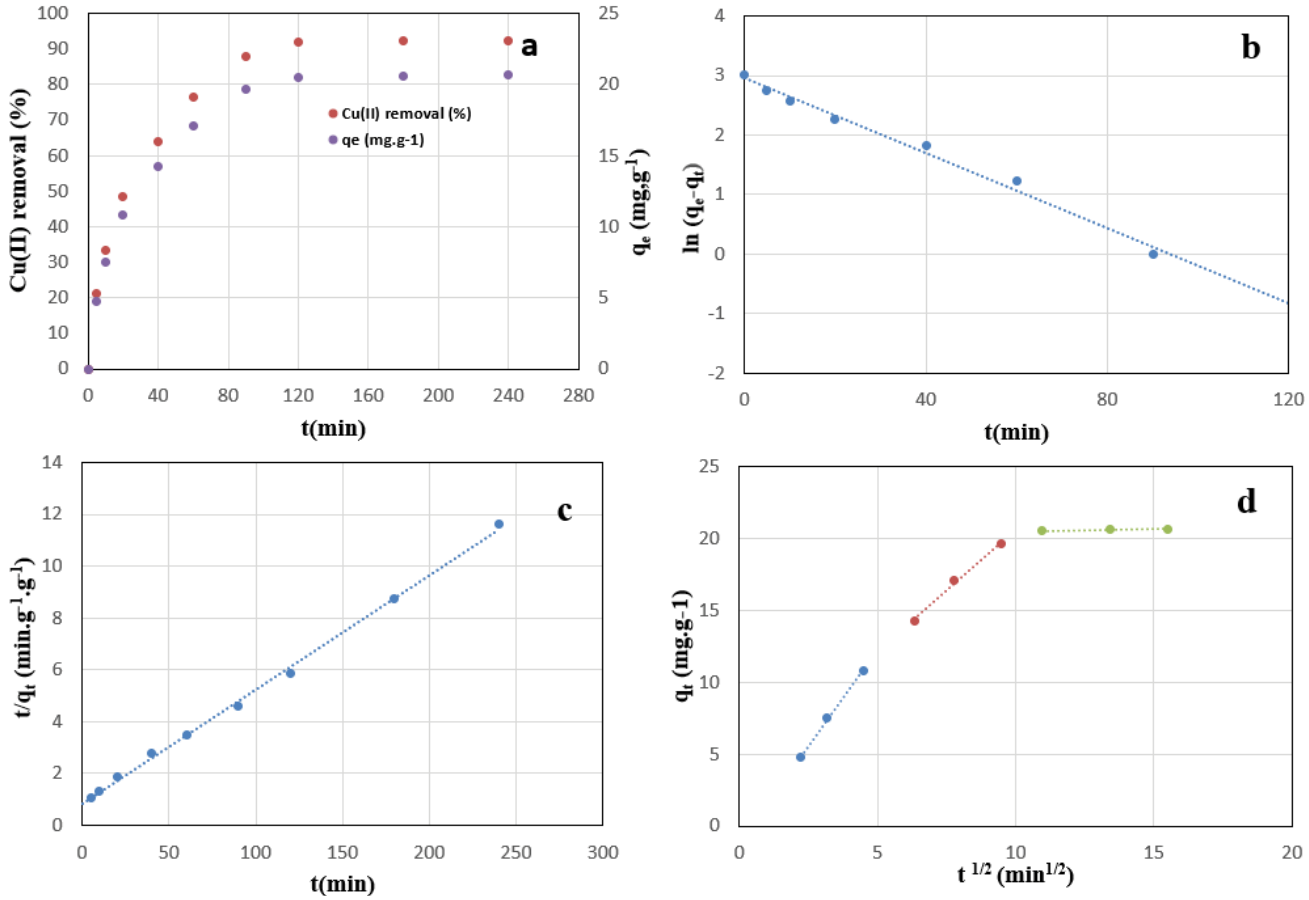


Fig. S1. Experimental data for the effect of reaction time (a), pseudo-first-order (b), pseudo-second-order (c) and intraparticle diffusion model (d) on Cu(II) adsorption.

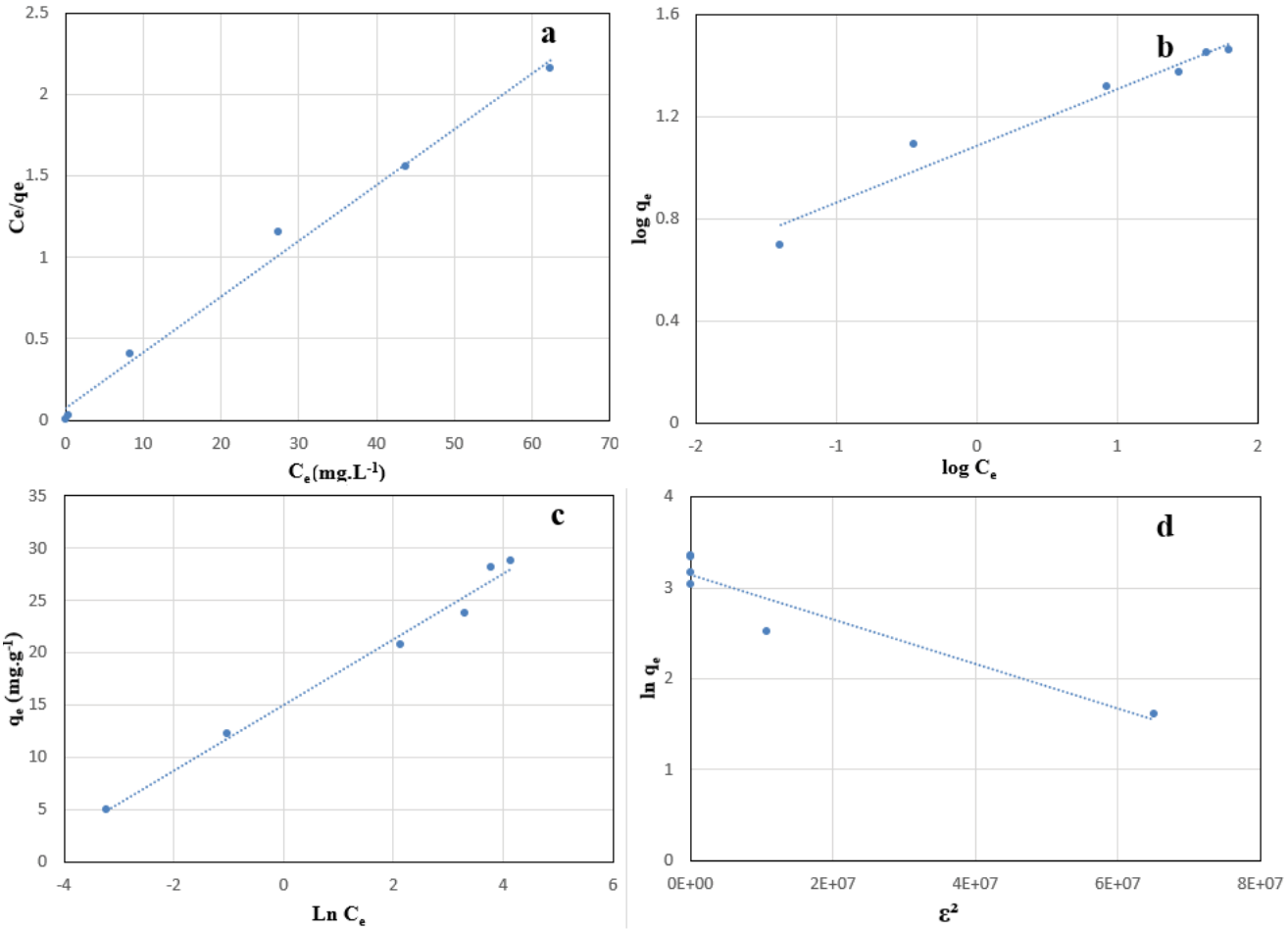


Fig. S2. Linear plots of Langmuir (a), Freundlich (b), Temkin (c) and Dubinin–Radushkevich (d) models for adsorption isotherms.

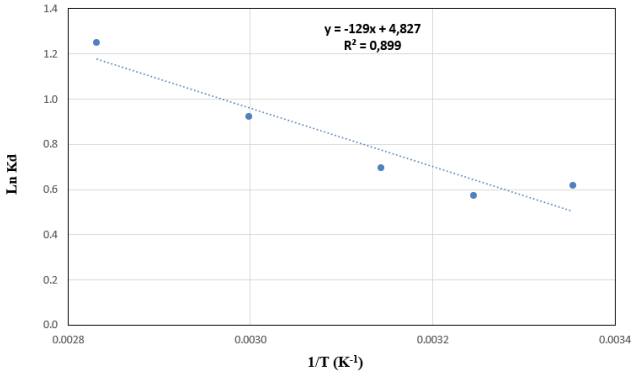


Fig. S3. Van't Hoff plot of ln$K_d$ vs. 1/$T$ for Cu(II) ions adsorption onto natural hydroxyapatite.